Mössbauer characterization of microbially mediated iron and manganese ores of variable geological ages

Maria Gracheva [a,*], Zoltán Homonnay [a], Krisztina Kovács [a], Kende Attila Béres [b], João Carlos Biondi [c], Yu Wenchao [d], Viktória Kovács Kis [e], Ildikó Gyollai [f], Márta Polgári [f,g]

[a] Institute of Chemistry, ELTE Eötvös Loránd University, 1117 Budapest, Pázmány Péter s. 1/A, Hungary
[b] Institute of Materials and Environmental Chemistry, Research Centre for Natural Sciences, ELKH, 1117 Budapest, Magyar Tudósok krt. 2, Hungary
[c] Federal University of Paraná State, Polytechnic Center, Geology Department, 81531-980 Curitiba, Brazil
[d] State Key Laboratory of Biogeology and Environmental Geology, School of Earth Sciences, China University of Geosciences, 430074 Wuhan, China
[e] Institute for Technical Physics and Materials Science, CER, Eötvös Loránd Research Network, 1525 Budapest, PO Box 49, Hungary
[f] Institute for Geological and Geochemical Research, RCAES, Eötvös Loránd Research Network, 1112 Budapest, Budaörsi u. 45, Hungary
[g] Eszterházy Károly University, Department of Natural Geography and Geoinformatics, 3300 Eger, Leányka u. 6, Hungary

ARTICLE INFO

ABSTRACT

A combination of various techniques was applied to investigate the mineralogy of the Neoproterozoic Urucum iron and manganese deposit (Brazil) and Carboniferous and Permian manganese carbonate deposits (China). The examined deposits exhibited signs of microbial mediation from Fe and Mn bacteria and cyanobacteria. The studied samples showed diversity in their composition and particle size. Probes from Urucum deposit revealed that the rocks consist mainly of hematite, showing Mn substitution which reflects the oxidation of Mn on the active surface of Fe-rich biomat. Nanominerals occurring in significant concentration also supported the microbial contribution to the formation of these ores. Representative samples of Neoproterozoic and Permian deposits showed considerable amount of mixed carbonates with variable composition.

[57]Fe Mössbauer spectroscopy analysis supported by X-ray diffraction and transmission electron microscopy data provided a detailed characterization of Fe-rich mineral phases of the samples, including metal ratio outlooks, particle size dimension and presence and type of impurities. Integrity and high resolution of the methods allowed to determine new features of the samples reflecting important signatures of microbial activity revealing the biogeochemistry of the biomat formation.

1. Introduction

[57]Fe Mössbauer spectroscopy is a powerful analytical tool applied in Earth science. It gives information about the Fe oxidation, spin and magnetic states of Fe and can be applied for both crystalline and amorphous Fe-containing compounds for which conventional diffraction methods fail (Kuzmann et al., 1998). Natural Fe oxides and (oxy-) hydroxides often deviate from ideal compositions due to poor crystallinity and isomorphous substitution, while Mössbauer spectroscopy is sensitive to these deviations due to rich spectral structure (Hassan, 2015).

The valence state and the coordination environment of Fe can be determined from the hyperfine parameters deduced from the analysis of the spectrum. Both qualitative and quantitative analysis of different iron components present in a mineral can be carried out without chemical destruction of the sample. Therefore, it is very fruitful to apply Mössbauer spectroscopy for characterizing rocks of magmatic, metamorphic and sedimentary origin and for the reconstructing processes of the rock formation. Fe^{3+}/Fe_{tot} ratios in the samples obtained from Mössbauer analysis could be used to constrain the oxygen fugacity of the rock and its evolution during crystallization of the magma (Cao et al., 2017).

A great advantage of Mössbauer spectroscopy compared to many other macroscopic techniques lies in the possibility to obtain magnetization orientation (Merkel et al., 2011, Tanczikó et al., 2009) and separate para-, ferro-, ferri-, and antiferromagnetic sub-lattices (Lipka, 1999). As opposed to magnetic susceptibility or magnetization measurements that summarize together contributions from all sources of

magnetism in the sample, Mössbauer studies are sensitive only to ^{57}Fe nuclei and cannot be affected by other component phases. Since the temperature of the magnetic transition may be particle size-dependent, by performing measurements of samples cooled down or heated up, in some cases the grain size of the Fe containing particles can be estimated (Johnson and Glasby, 1969; Gracheva et al., 2017).

The possibility of applying different values of temperature and pressure on the sample makes Mössbauer spectroscopy a priceless way to study the crystal chemistry of Fe in the lower mantle where the dominant components are ferropericlase (MgFe)O (Lin et al., 2009) and perovskite (Mg,Fe)SiO$_3$ (McCammon et al., 2008), and in the Earth core (Bessas et al., 2020a, 2020b).

To exclude most of impurities, application of Mössbauer spectroscopy to investigate biomineralization processes was mostly performed with living microorganisms and under laboratory conditions. This technique has been used as a basic tool to study magnetotactic bacteria and precipitated magnetite produced by them (Frankel and Blakemore, 1984), and to describe biotransformations of minerals by iron-reducing bacteria (Zavarzina et al., 2020).

Research made on Neoproterozoic Urucum manganese deposit interbedded in banded iron formation in Brazil (Biondi and Lopez, 2017, Biondi et al., 2020) and on manganese carbonate deposit in China (Yu et al., 2019) concluded that these sedimentary ore formations of variable geological ages are microbialite. The banded iron formation was also interpreted on the basis of multi-methodological complex investigations (Polgári et al. 2021, submitted to this thematic volume).

Various Fe minerals (real Fe ore minerals like hematite, pyrite, siderite) and Fe-bearing minerals (like Fe-bearing silicates like celadonite, aegirine, Fe-bearing carbonate like ankerite) (Fe minerals hereafter) are main or basically important components of these ores (even the Mn ores contain Fe minerals and Fe-bearing minerals in lower amount), and these Fe minerals also represent paleoenvironmental information on formation conditions, including Eh, pH and microbial contribution. The determination of Fe minerals was made by high

resolution, sensitive *in situ* Fourier-transform infrared spectroscopy (FTIR) and Raman spectroscopy and the results of the studied ore deposits are summarized in Table 1. The excitation energy of Raman laser is higher, than infrared energy, and caused transformation of poorly crystallized Fe minerals, like ferrihydrite to goethite, hematite.

The microbialite samples, in general, are fine grained (0.5–1 μm dimension) and contain variable organic matter embedded. The Fe-oxide-hydroxides include syngenetic poorly crystallized ferrihydrite and lepidocrocite, which are the result of direct microbial Fe(II) oxidation under suboxic, semineutral conditions. The stabilized crystal forms also occur as hematite and goethite. Magnetite, mixed Fe(II)/Fe(III)-oxide, reflects suboxic heterotrophic microbial mediation (Frankel and Blakemore, 1984; Polgári et al., 2019). Fe-bearing anatase represents a special mineral phase in the deposits, occurring similarly in mineralized microbially formed cycles, biomats. Jacobsite, a Mn-Fe-bearing oxide, refers to combined microbially mediated mineralization of Mn and Fe, also in cyclic form.

After burial, during diagenesis, the decomposition of organic matter and mineralization of organic carbon to carbonates result in the formation of siderite and mixed carbonates, like ankerite. Combination of Fe-oxide and segregated silica with cations released via decomposition of organic matter yields Fe-bearing silicates, like aegirine, and clay minerals, celadonite (Fe mica) and nontronite (Fe-smectite). When diagenesis reaches anoxic conditions, pyrite, marcasite and Na-jarosite precipitate. Pyrite and marcasite also form mineralized biomat cycles.

The formations studies are natural processes, so the effect of contamination, impurities probably make the interpretation of the result more complicated.

The results of investigation of Carboniferous and Permian manganese carbonate deposits of China are submitted also to the recent volume as individual manuscripts. Geological background, sampling locations and sample descriptions are given by Yu et al. (2021a), Yu et al. (2021b) and Polgári et al. (2021) submitted to recent volume.

The aim of this paper is the characterization of Fe minerals of these

Table 1

Fe minerals* of black shale-hosted manganese carbonate ore deposits of China (Masi, Xinglong), and banded iron formation Urucum, Brazil, and their paleoenvironmental consideration.

Minerals/ Processes	Chemical formula	Brazil Urucum[1]	China Masi[2]	China Xinglong[3]	Eh			pH			Microbially mediated
					oxic	subox	anox	acidic	neutral-slightly alkaline	alkaline	
Fe mineral assemblage											
Oxides and hydroxides											
Ferrihydrite	$Fe_5O_8H \cdot 4(H_2O)$	*	*	*		*			*		*
Lepidocrocite	$\gamma\text{-}FeOOH$		*	*		*			*		*
Hematite	$\alpha\text{-}Fe_2O_3$	*	*	*	*						
Goethite	$\alpha\text{-}FeOOH$	*	*	*		*					
Magnetite	Fe_3O_4			*		*			*		*
Anatase	$TiO_2 - Fe_xTi_{(1-x)}O_{(2-x)}OH_x$	*	*	*		*			*		*
Jacobsite	$Mn^{2+}_{0.6}Fe^{2+}_{0.3}Mg_{0.1}Fe^{3+}_{1.5}Mn^{3+}_{0.5}O_4$	*	*	*	*						
Carbonates											
Siderite	$FeCO_3$	*	*	*		*					*
Ankerite	$Ca(Fe^{2+},Mg)(CO_3)_2$	*		*		*					
Silicates											
Aegirine	$Ca_{0.75}Na_{0.25}Mg_{0.5}Fe^{2+}_{0.25}Fe^{3+}_{0.25}(Si_2O_6)$	*		*		*				*	*
Nontronite	$Na_{0.3}Fe^{3+}_2Si_3AlO_{10}(OH)_2 \cdot 4(H_2O)$		*				*		*		*
Celadonite	$KMg_{0.8}Fe^{2+}_{0.2}Fe^{3+}_{0.9}Al_{0.1}Si_4O_{10}(OH)_2$		*			*			*		*
Sulfides											
Pyrite	FeS_2		*	*			*	*			*
Marcasite	FeS_2	*		*			*	*			*
Sulphates											
Na-jarosite	$NaFe^{3+}_3(SO_4)_2(OH)_6$		*	*			*	*			*
Organic material		*	*	*							*

*Fe minerals and Fe-bearing minerals.
[1] : Polgári et al. (2021) submitted to OGR special issue
[2] : Yu et al. (2021a) submitted to OGR special issue.
[3] : Yu et al. (2021b) submitted to OGR special issue.

ore deposits by Mössbauer spectroscopy, with special interest on bio-mineralization. Mössbauer investigations not only support the results obtained by other technique but also provide precise integral information about Fe mineral occurring in the sample, particle size, effect of impurities and magnetization properties. Formation model of deposits is interpreted as microbialites based on complex datasets.

2. Samples and methods

2.1. Samples

The samples were collected in operating mines (Yu et al., 2021a, 2021b; Polgári et al., 2021 submitted to OGR special issue). The list of samples and the used methods are summarized in Table 2.

2.2. Methods

To investigate iron compounds present in the samples, ^{57}Fe Mössbauer spectroscopy measurements were performed on powdered bulk samples (with randomly oriented grains to avoid any texture effects in the spectrum evaluations) at room temperature and at $T = 80$ K, using a conventional Mössbauer spectrometer (WissEl) operating in the constant acceleration mode with ^{57}Co source in Rh matrix (ELTE, Budapest, Hungary). For low temperature measurements the samples were kept in a cryostat (SVT-400-MOSS, Janis) filled with liquid nitrogen.

The Mössbauer spectra were evaluated by standard computer-based statistical analysis methods that included fitting the experimental data by a sum of Lorentzians using a least-squares minimization procedure with the help of the MossWinn 4.0 program (Klencsár et al., 1996). The isomer shifts are given relative to α-Fe at room temperature.

The mineral composition was determined by X-ray powder diffraction (XRD) analysis on a Philips PW 1050 instrument in the Research Centre for Natural Sciences, ELKH (Budapest, Hungary) using the CuKα radiation ($\lambda = 0.15418$ nm) generated by setting the tube voltage and the current to 40 kV and 35 mA respectively. The patterns were taken in the Bragg–Brentano geometry in the angle range of 4–70° with 0.04°/s scanning rate. Lattice parameters were calculated by fitting peaks with Voigt functions.

The morphology and crystallinity of the representative samples were checked using transmission electron microscopy (TEM) and the composition was followed by means of energy dispersive spectroscopy (EDS) in the Institute for Technical Physics and Materials Science, CER (Eötvös Loránd Research Network, Budapest, Hungary). Suspension samples for the TEM analysis were prepared using ethanol. A drop of the resulting suspension was deposited onto lacey carbon coated copper TEM grid (Ted Pella). TEM analysis was performed at 200 keV accelerating voltage using an FEI Themis 200 G3 TEM with a C_s corrected objective lens (FEG, point resolution is around 0.09 nm in HREM (High Resolution Electron Microscope) mode and 0.16 nm in STEM (Scanning Transmission Electron Microscope) mode) equipped with FEI Super-X EDS detection 182 system.

3. Results

Mössbauer spectral characterization of 20 samples was performed on 27 spectra. Four samples were chosen for additional XRD analysis and TEM investigation.

3.1. Urucum – banded iron formation – Fe ore microbialite with Mn mineralized biomat system

All Mössbauer spectra of the investigated samples from the Urucum mine are dominated by magnetic sextets of octahedrally coordinated Fe (III) (Fig. 1). The hyperfine parameters (isomer shift $\delta = 0.35(1)$ mm/s, quadrupole shift $2\varepsilon = -0.20(1)$ mm/s, hyperfine magnetic field $B_{hf} = 51.5(5)$ T) remain almost the same in all cases and correspond to Fe

Table 2
List and description of studied samples.

Sample	Description*	Location	MS at RT	MS at $T = 80$ K	XRD	TEM-EDS
COR-86	The rock samples are massive red and metalliferous dark gray, black, fine to coarse grained, laminated and noduliferous representative BIF ore samples at Urucum[1]	Urucum, Brazil	*			
COR-87			*			
COR-88			*			
COR-88			*			
COR-93			*			
COR-97			*			
COR-120			*			
COR-127			*	*		*
COR-133			*			
COR-137			*	*		
COR-141			*	*	*	*
COR-151			*	*		
COR-152			*			*
COR-153A			*			
COR-153B			*	*	*	
COR-157			*			
COR-168			*	*	*	*
MS-2	Massive dark gray, black, fine grained representative Mn carbonate ore sample, finely laminated with pyrite laminae[2]	Masi, Central Guangxi, South China	*	*	*	
XL-4	Massive dark gray, black, fine to coarse grained representative Mn carbonate ore sample with diagenetic sedimentary features, without macroscopically visible lamination[3]	Xinglong, North Guizhou, South China	*			
XL-5			*			

Abbreviations: BIF – banded iron formation, MS – Mössbauer spectroscopy, RT – room temperature, XRD – X-ray powder diffraction, TEM-EDS – transmission electron microscopy with energy dispersive spectroscopy
*Detailed geological information is in [1]: Polgári et al. (2021) submitted to OGR special issue; [2]: Yu et al. (2021a) submitted to OGR special issue; [3]: Yu et al. (2021b) submitted to OGR special issue

nuclei in the hematite Fe_2O_3 structure. However, precise evaluation of the sextet revealed various values for the difference between the line width of the first and the third lines. Depending on this value all samples were classified rather arbitrarily into three groups: small (line width difference below 0.07 mm/s), medium (0.08–0.13 mm/s) and big (more than 0.14 mm/s). This line width difference is assigned to hyperfine field distribution (Table 3). The highest linewidth difference 0.21 mm/s was observed in the case of sample COR-168.

In a few cases (COR-127, COR-137, COR-141, COR-151, COR-153B) a broad Fe(III) relaxation component is observed in the middle of the spectrum (Fig. 2). It can correspond to paramagnetic phases of iron
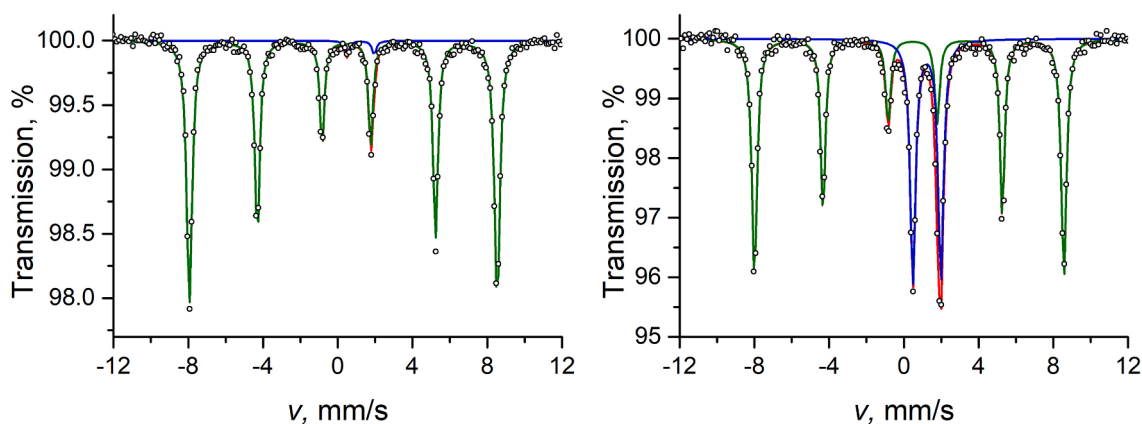
Fig. 1. Mössbauer spectra of the samples COR-87 (left) and COR-152 (right) measured at room temperature.

Table 3
Fe minerals* in the Urucum samples.

Sample	Bulk hematite Fe$_2$O$_3$	Mixed Fe carbonates	Others
COR-86	90.4(4)% HFD	9.6(4)%	–
COR-87	98.0(5)% HFD	2.0(5)%	–
COR-88	90.1(5)% HFD	9.9(5)%	–
COR-93	86.3(7)% MFD	13.7(7)%	–
COR-97	94.0(5)% MFD	6.0(5)%	–
COR-120	100% HFD	–	–
COR-127	84.0(5)% SFD	–	16.0(5)% nanohematite
COR-133	100% SFD	–	–
COR-137	90.5(5)% SFD	–	1.2(3)% bixbyite 8.3(8)% nanohematite
COR-141	94.2(5)% SFD	–	5.8(5)% nanohematite
COR-151	74.3(5)% SFD	7.9(5)%	17.8(5)% nanohematite
COR-152	65.6(6)% SFD	34.4(6)%	–
COR-153A	99.0(5)% MFD	1.0(5)%	–
COR-153B	70.2(5)% SFD	–	22.1(5)% jacobsite 4.8(3)% nanohematite 2.9(3)% bixbyite*
COR-157	90.4(5)% MFD	9.6(5)%	–
COR-168	100% HFD	–	–

Abbreviations: SFD – small field distribution, MFD – medium field distribution, HFD – high field distribution, see text for the determination explanation; *bixbyite – (Mn,Fe)$_2$O$_3$.
*Fe minerals and Fe-bearing minerals.

hydroxides (ferrihydrite/lepidocrocite) or to small particles of magnetic phases (hematite/goethite). Taking into account that all ferric oxy-hydroxides or hydrous oxides have very close Mössbauer parameters at room temperature, measurements of these samples were performed at low temperature. At $T = 80$ K the broad component observed earlier either disappeared (COR-127, COR-137, COR-151) or broadened and decreased (COR-141, COR-153B).

Upon cooling down below $T_M \sim 255$ K, hematite undergoes magnetic phase transition (known as Morin transition) that can be seen in the spectrum by the change of the sign of the quadrupole shift value from $2\varepsilon = -0.20$ mm/s to $2\varepsilon = 0.30$ mm/s. The quadrupole interaction shifts the inner 4 lines of the sextet relative to the outer 2 lines. Among the low temperature measurements, Morin transition and corresponding change in the relative line positions were observed in the case of samples COR-127 (Fig. 3), COR-151 and COR-153B. Such change was not observed at $T = 80$ K in the case of COR-137 and COR-141.

Fe(II) high spin compounds usually appear in Mössbauer spectra as sharp doublets with high isomer shift and quadrupole splitting values (see the blue subspectrum in Fig. 1). Such components are present only

in some samples and can be identified as mixed Fe(II) carbonates. Due to the observed quadrupole splitting values ($\Delta = 1.44–1.50$ mm/s) which are substantially lower than that for regular siderite FeCO$_3$ ($\Delta = 1.86$ mm/s (Stevens et al., 1998)), the doublet should rather correspond to ankerite Ca(Fe,Mg)CO$_3$ or other carbonate mineral with Fe impurity.

From the series, only two spectra (of samples COR-137 and COR-153B) exhibited the presence of a very special doublet ($\delta = 0.39(1)$ mm/s, $\Delta = 1.32(2)$ mm/s). This relatively high quadrupole splitting for Fe(III) can rarely be observed in natural minerals and is very typical for bixbyite (Mn,Fe)$_2$O$_3$ (S.N. de Medeiros et al., 2004). However, the quality of the low temperature spectrum doesn't allow to resolve bixbyite component, because its relative area is too small and cannot be identified behind the broad relaxation subspectrum.

Besides hematite and bixbyite components the spectrum of COR-153B sample contained another sextet. Zero quadrupole shift with smaller magnetic hyperfine field ($B_{hf} = 40.2$ T) suggests that this sub-spectrum cannot correspond to hematite particles. Additional low temperature Mössbauer measurements showed that this component can be identified as jacobsite MnFe$_2$O$_4$.

Based on the Mössbauer data obtained the ratio of different iron mineral phases observed in the samples is summarized in Table 3.

To confirm Mössbauer results three samples COR-141, COR-153B and COR-168 from Urucum mine were investigated by means of X-ray powder diffraction (Fig. 4). In all cases, the calculated lattice parameters of hematite are slightly different from the standard (Table 4) suggesting some distortion. Besides hematite, both COR-141 and COR-168 exhibited significant quartz SiO$_2$ peak in the pattern. In COR-153B quartz concentration is below the detection limit but the presence of bixbyite and jacobsite observed in the Mössbauer spectrum was confirmed by XRD experiment. Carbonates were observed in the case of COR-153B and COR-168 in the form of dolomite CaMg(CO$_3$)$_2$ and calcite CaCO$_3$ respectively.

In order to investigate the substitutions in Fe phases, TEM-EDS measurements were performed on the representative samples COR-127, COR-141, COR-152 and COR-168. SAED patterns and EDS spectra exhibited the presence of pure hematite without any impurities for both COR-127 (Fig. 5) and COR-152. The perfectly ordered structure of hematite can be seen on the HRTEM image. In contrast, hematite in COR-141 sample contained small amount of Mn (Fig. 6, left). Moreover, typically small particles (50–100 nm) of Mn oxides with elongated morphology were detected besides the large particles in this sample (Fig. 6, right). In addition to hematite, intensity distribution of the EDS signal of COR-152 sample indicates that the Fe is incorporated into the carbonate structure (Fig. 7). Quantitative analysis of the spectrum collected from the area indicated on the High Angle Annular Dark Field (HAADF) image is presented in Table 5. The composition, (Fe + Mg):Ca = 1:1, proves the presence of ankerite. In all three samples described above some Fe free clay minerals were detected. Unlike others, COR-168
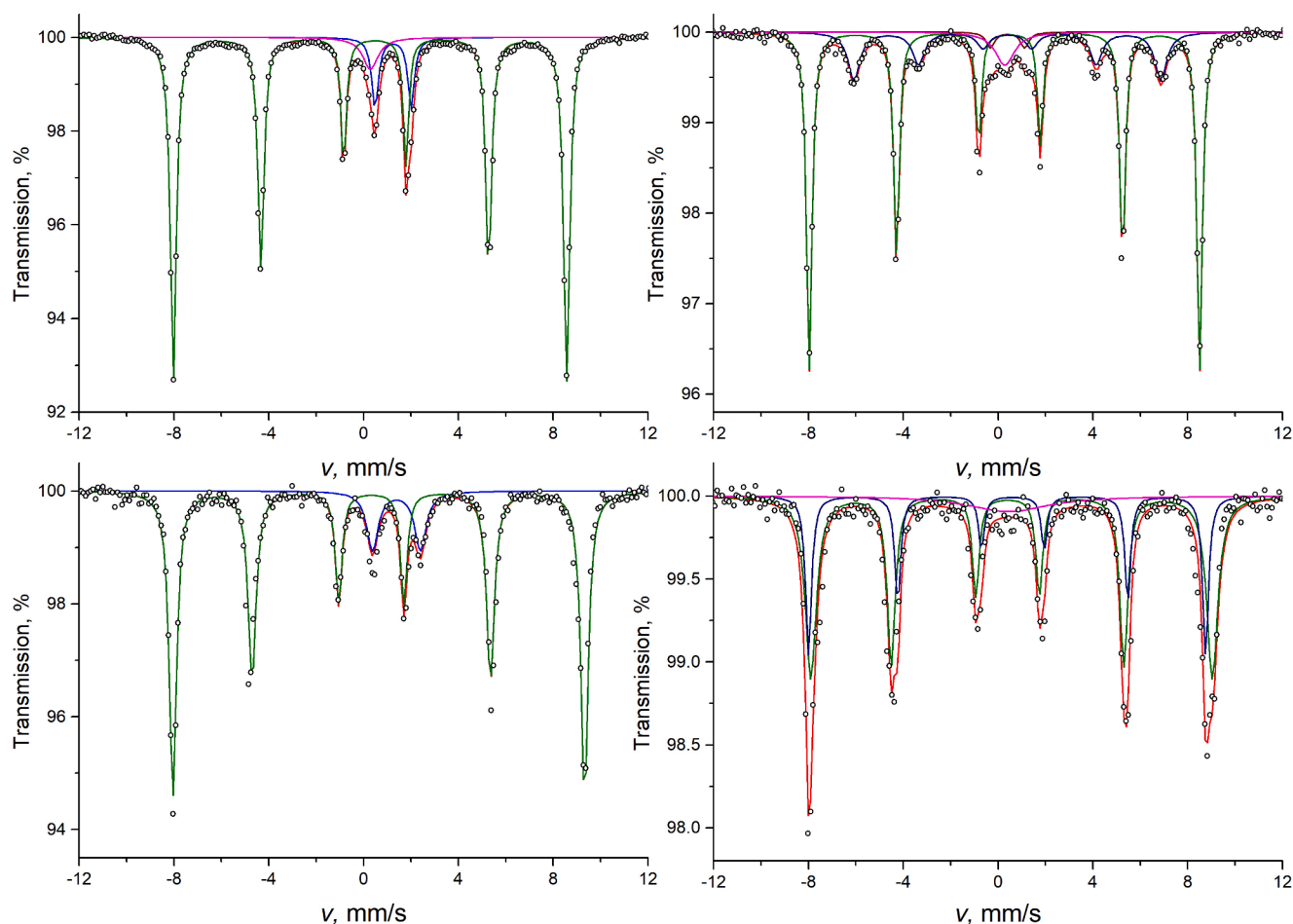
Fig. 2. Mössbauer spectra of the samples COR-151 (left) and COR-153B (right) measured at room temperature (top) and at $T = 80$ K (bottom).

proved to be free of clay minerals but exhibited a significant amount of calcite. Despite expectations (to account for the big difference in line widths within the sextet of hematite), no observable substitution (Al, Mn, Mg or Si) was detected in hematite structure in this sample.

3.2. China – Carboniferous Mn carbonate ore microbialite with Fe mineralized biomat system

Chinese Mn carbonate deposits are Fe poor (also based on the chemical analysis (Yu et al., 2021ab). The room temperature spectrum of MS-2 sample consists of only one sharp and nicely resolved doublet with parameters $\delta = 0.31(1)$ mm/s, $\Delta = 0.60(1)$ mm/s, line width $\Gamma = 0.25(1)$ mm/s which can be assigned to Fe(II) in a low spin state in a sulfur surrounding (Fig. 8, left). This spectrum can correspond to pyrite or marcasite (Shiley et al., 1981). Low temperature measurements exhibited also the presence of only one doublet. Despite the Raman results, suggesting the presence of siderite and ferrihydrite, additional XRD experiment (Fig. 4) confirmed the presence of pyrite (Table 6) and absence of any other Fe containing phase including marcasite. Other minerals detected in the pattern are hausmannite Mn_3O_4 and quartz.

3.3. China – Permian Mn carbonate ore microbialite with Fe mineralized biomat system

In the Permian samples XL-4 and XL-5 Fe content was even smaller which influenced the quality of the spectra (Fig. 8, right). The fitting model consisted of two quadrupole doublets. As in the previous case, only Fe(II) components were detected. The quadrupole doublet with a smaller isomer shift ($\delta = 0.29(1)$ mm/s, $\Delta = 0.59(2)$ mm/s, $\Gamma = 0.27(1)$

mm/s) corresponds to low spin Fe(II) surrounded by sulfur (pyrite, marcasite). The component with a higher isomer shift ($\delta = 1.26(1)$ mm/s, $\Delta = 1.70(1)$ mm/s, $\Gamma = 0.38(1)$ mm/s) corresponds to Fe(II) containing carbonate.

4. Discussion

4.1. Urucum – banded iron formation – Fe ore microbialite with Mn mineralized biomat system

Mössbauer analysis of the representative samples proved the prevalence of hematite as the stabilized form of Fe. The presence of sharp and nicely resolved six lines in all spectra even at room temperature suggests that the hematite particles are mostly bulk (more than 30 nm in diameter) (Dormann et al., 1989). The observed variation in the line width values of the hematite sextet exhibits some magnetic hyperfine field distribution. Correlation of these parameters with the degree of substitution was observed earlier (Murad and Schwertmann, 1986) and reflects impurities in the lattice.

The small difference between the line width values suggesting negligible field distribution and low amount of substitutions in hematite was confirmed in the case of COR-127, COR-151 and COR-153B. It was also supported by the observation of the Morin transition at T greater than 80 K in these samples and by results of TEM-EDS analysis.

If the transition is not observed at $T = 80$ K as in the case of COR-137 and COR-141, it is also an indication of impurities (it was described earlier for Mn and Al (Srivastava and Sharma, 1972; Vandenberghe et al., 1986). From this point of view, these two samples are controversial because the small line width difference indicates minor
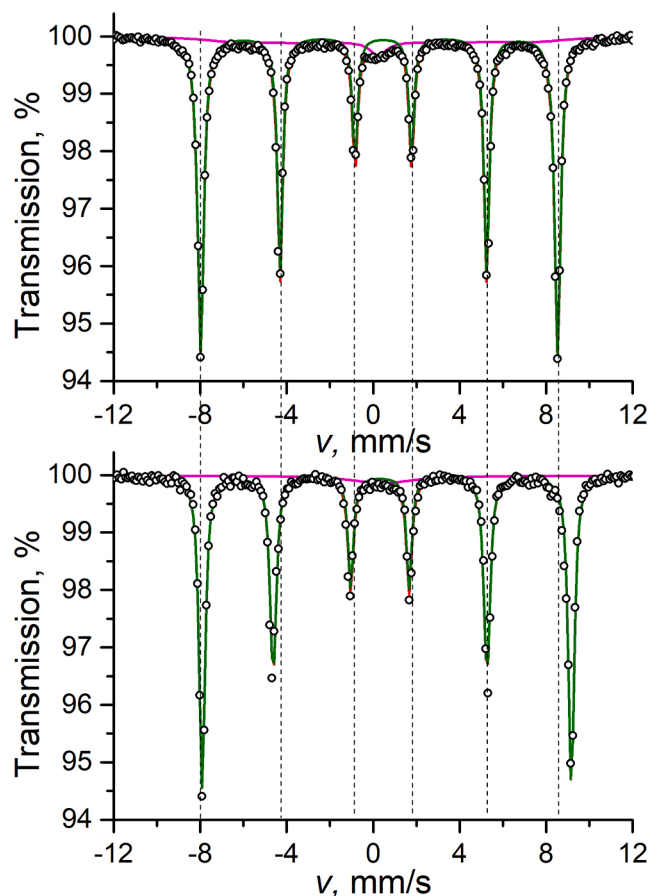
Fig. 3. Mössbauer spectra of the samples COR-127 measured at room temperature (top) and at $T = 80$ K (bottom).

impurities, while the Morin transition is still missing. In contrast,

hematite in the sample COR-168 exhibiting the biggest linewidth difference and supposing to have the largest amount of impurities, undergoes Morin transition at T greater than 80 K which is supposed to be suppressed by substitutions. In all cases the calculated lattice parameters of hematite are slightly different from the standard (Table 4) suggesting some distortion. Such contradiction can be explained by different types of impurities in hematite in various samples.

Mn substitution in hematite was confirmed by means of TEM-EDS technique for COR-141 suggesting that in this series of samples the lack of Morin transition is the sign of Mn atoms in hematite structure. Mn impurity in the Fe oxide minerals supports catalytic oxidation of Mn (II) to Mn(III, IV) on active surface (Morgan, 2005) as the latter can substitute directly for Fe(III) in the lattice of hematite. In this case the active surface is supposed to have been produced by the microbially mediated direct Fe oxide (biomat) formation. Another remarkable feature is the observation of small (less than 100 nm) Mn oxide particles attached to the bulk hematite in COR-141. According to the elemental ratio obtained by EDS analysis, the most possible compound is hausmannite. However, XRD pattern exhibit no presence of Mn phases in the sample. A possible explanation of this phenomenon is that either the amount of these particles is too low for XRD detection, or they are XRD amorphous.

However, the absence of any substitute elements in COR-168, despite the highest field distribution observed in its Mössbauer spectrum, remains unclear. TEM-EDS showed only the presence of Fe, O and Ca in the samples, where the latter two are associated to calcite. A suitable explanation for this contradiction can be organic impurity. Small

Table 4

Lattice parameters of hematite revealed from XRD analysis.

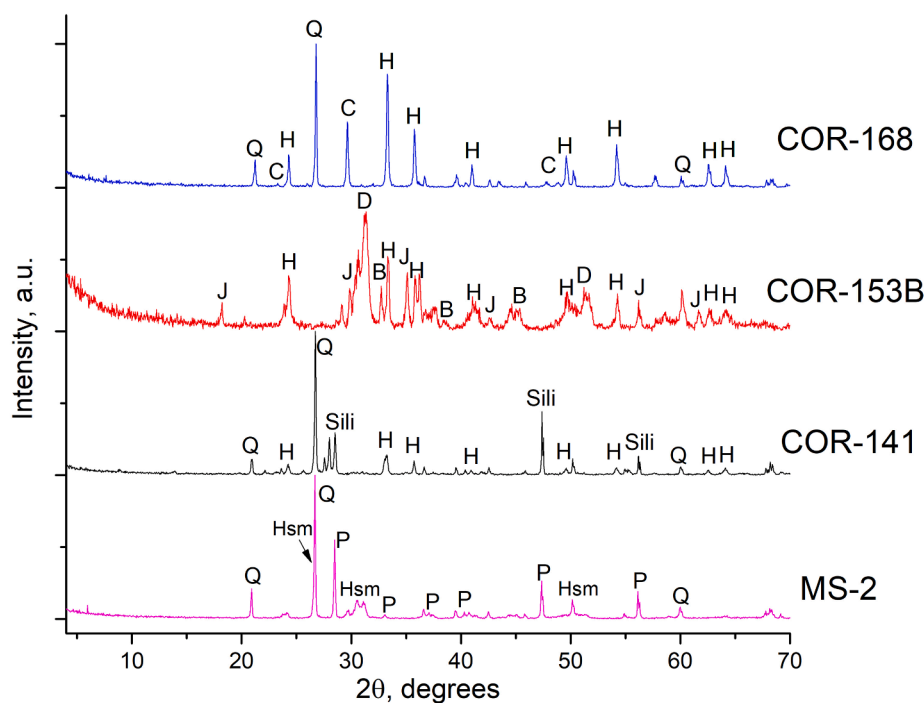| Sample	$a = b$, Å	c, Å
Standard Fe$_2$O$_3$*	5.040	13.78
COR-141	5.031(2)	13.71(1)
COR-153B	5.016(2)	13.69(2)
COR-168	5.021(4)	13.73(2)

* Weihe et al. (2019).

Fig. 4. Normalized X-ray diffraction patterns for COR-141, COR-153B, COR-168 and MS-2, abbreviations: B – bixbyite, C – calcite, D – dolomite, H – hematite, J – jacobsite, P – pyrite, Q – quartz, Sili – silicon added to COR-141 and MS-2 to determine the shift.
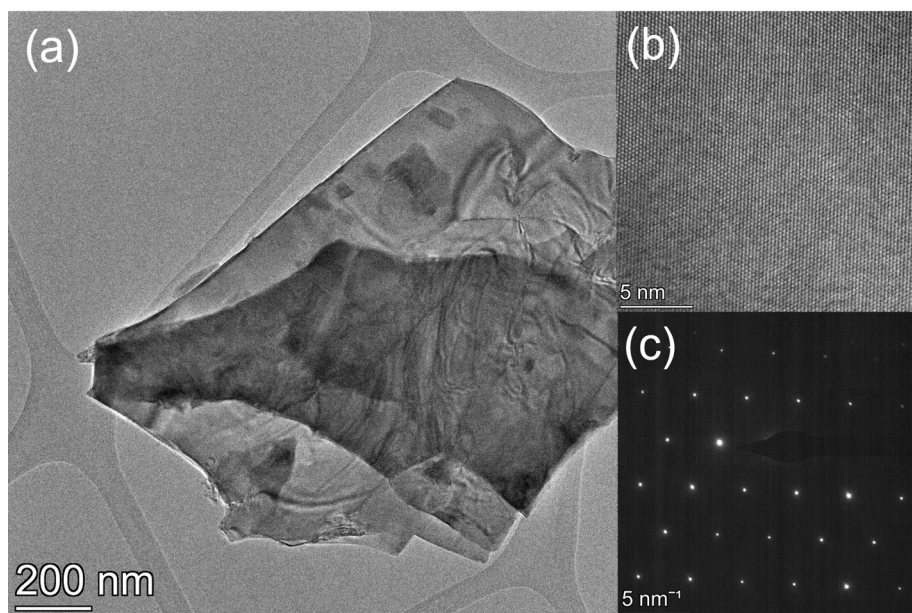
Fig. 5. Bright field TEM image (a), high resolution image (b) and selected area electron diffraction pattern (c) of a hematite particle in [0 0 1] zone axis projection in the COR-127 sample.
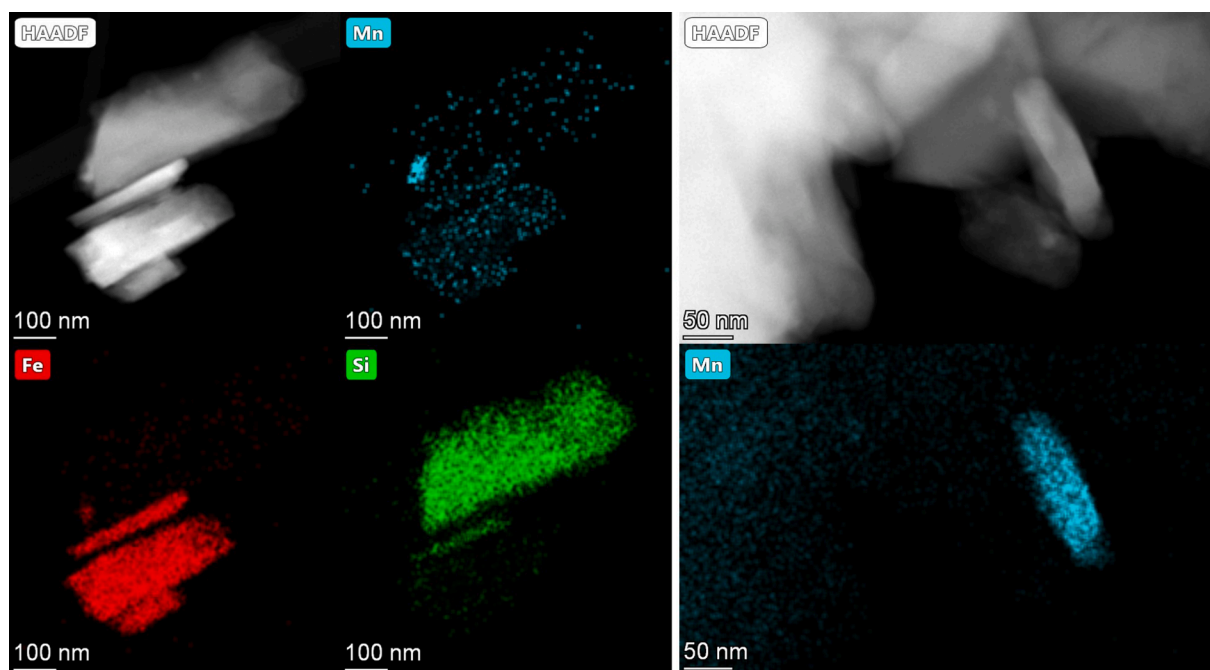

Fig. 6. STEM HAADF images and corresponding elemental maps of different aggregates observed in COR-141.

organic anions might incorporate into the hematite structure, while their presence is impossible to detect by diffraction methods (Lenhart et al., 2010; Weihe et al., 2019). It can be assumed that in this series of samples the field distribution correlates with the organic material substitution in the hematite structure. Organic matter impurities support syngenetic microbial activity, and decomposition of these components, which were embedded into the forming Fe oxide mineral phases during their formation.

The presence of Fe(II) in the form of ankerite in some samples fits well with electron probe microanalyzer studies, that ankerite is a common constituent in the samples with variable composition (mixed carbonates), and it supports microbially mediated complex early diagenetic

mineralization. According to Reeder and Dollase (1989), the increase of the Fe content in dolomite and ankerite causes octahedral distortion and results in lower quadrupole splitting values. Quadrupole splitting in samples COR-93, COR-151, COR-152 and COR-153A corresponds to Fe molar fraction of less than 0.3, while in samples COR-87, COR-88, COR-97, to Fe molar fraction of more than 0.5. In the case of COR-86 and COR-157 data suggest that around 40% of the B site in ankerite is occupied by Fe. These calculations are supported by metal ratio found in COR-152 by means of TEM-EDS. The presence of ankerite also fits the cathodoluminescence features of the samples (Polgári et al., 2021 submitted to this thematic volume).

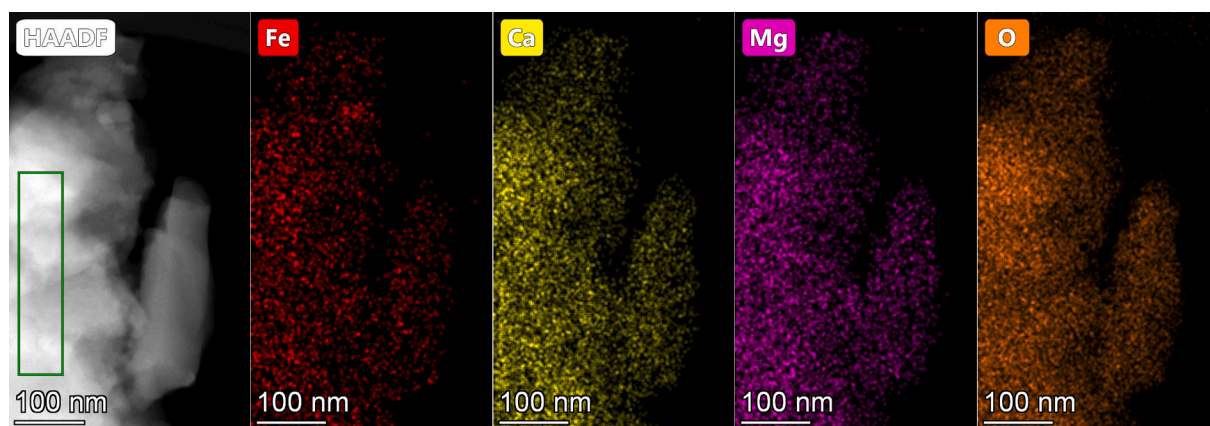The temperature behavior of the relaxation component reflects the

Fig. 7. STEM HAADF images and corresponding elemental maps of an aggregate in COR-152.

Table 5
Quantitative analysis of the energy dispersive spectrum obtained for COR-152.

Z	Element	Atomic Fraction, %	Atomic Error, %	Mass Fraction, %	Mass Error, %	Fit error, %
8	O	75.39	5.89	57.80	3.14	3.19
12	Mg	9.32	1.97	10.85	2.21	1.64
20	Ca	12.67	1.91	24.34	3.41	0.28
26	Fe	2.62	0.40	7.01	0.98	0.76

presence of nanohematite particles of different size. In the case of total disappearance of this component (COR-151, Fig. 2, left) the particle size lies in a range between 10 and 30 nm, if the component remains but broadens (COR-153B, Fig. 2, right) the particles diameter is even less than 10 nm (Bødker and Mørup, 2000). The presence of such small particles cannot be caused by sample grinding during preparation. Size dimension of hematite crystals in the few tens of nm refers also to microbial mediation, since in these cases, the formation of larger crystals is inhibited by organic films (Konhauser, 1998; Pédrot et al., 2011).

Jacobsite was determined by FTIR and Raman spectroscopies (Table 1), and was interpreted as a combined Fe-Mn oxide, which occur in mineralized cycles, representing mineralized Fe biomats. It is

remarkable that in contrast to Ashokan et al. (1988), the jacobsite observed in the Mössbauer spectrum of COR-153B contains only Fe(III) component, no Fe(II) substitution was detected. However, the Mössbauer parameters obtained are in good agreement with those already observed for jacobsite $MnFe^{3+}_2O_4$ in manganese ores previously reported (da Costa and Herzog, 2011).

4.2. China – Carboniferous Mn carbonate ore microbialite with Fe mineralized biomat system

Pyrite and marcasite observed earlier in Raman spectra have very close hyperfine parameters (Stevens et al, 1998.) and can hardly be distinguished based on Mössbauer spectra. However, XRD also showed no detectable amount of other Fe containing minerals besides pyrite.

Table 6
Fe minerals* in the samples from Chinese deposits.

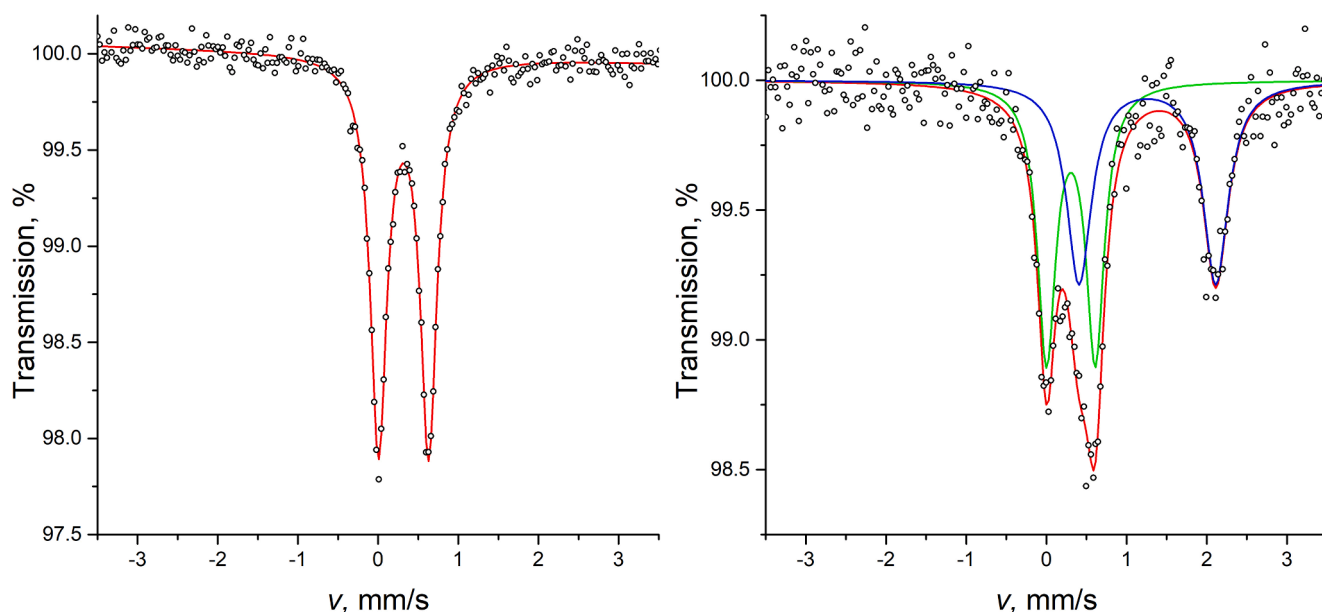| Sample	Pyrite FeS_2	Mixed Fe carbonates
MS-2	100%	–
XL-4	20(1)%	80(1)%
XL-5	50.1(8)%	49.9(8)%

*Fe minerals and Fe-bearing minerals.

Fig. 8. Mössbauer spectra of the samples MS-2 (left) and XL-5 (right) measured at room temperature.

Moreover, small width of both Mössbauer and XRD lines suggests hardly any distortion in the Fe microenvironment and reflects the presence of Fe in only pure pyrite structure without any detectable contaminations. Hausmannite was not distinguished earlier in Raman and IR experiments. It might be connected to the similarity of some different manganese oxides in Raman spectra (Bernard et al., 1993). Furthermore, hausmannite is a typical sign of sample degradation upon heating (Zaki et al., 1997), so its appearance in the spectrum might be connected to the laser-induced transformations.

4.3. China – Permian Mn carbonate ore microbialite with Fe mineralized biomat system

Low spin Fe(II) component has very close parameters to the one observed in the Carboniferous samples XL-4 and XL-5. Therefore, it can be also identified as pyrite. The sharp lines of this doublet suggest that the amount of impurities in the FeS_2 structure is negligible as previously.

Based on the literature data (Shiley et al., 1981), it was concluded that the component with a higher isomer shift corresponds to Fe(II) carbonate, mostly in the form on ankerite $Ca(Fe,Mg)(CO_3)_2$ (Table 6), which fit well with recent studies Yu et al., 2021b (this volume). The parameters of the carbonate ($\Delta = 1.69(1)$ mm/s) are slightly different from those reported for pure siderite ($\Delta = 1.86$ mm/s) but Δ is not as low as we observed in the case of Urucum samples ($\Delta = 1.44$–1.50 mm/s). Such value of the quadrupole splitting suggests that Fe octahedra is more distorted than it was observed in Urucum samples and probably most of the B sites are occupied by Mg. However, the broad line of this sub-spectrum reflects the presence of slightly different Fe microenvironments, probably due to the minor variations of the interatomic distances Fe-O in the ankerite particles.

5. Conclusion

We applied ^{57}Fe Mössbauer spectroscopy, XRD and TEM EDS techniques to investigate Fe minerals of natural, sedimentary, microbialite Fe and Mn ores of different localities and various geological ages. The major conclusions of the study are summarized as follows:

- For all representative samples the mineral composition was determined. In the case of Urucum deposit, the most abundant Fe form was hematite. In the samples from Chinese deposits Fe occurred only in the ferrous form. The Carboniferous probe showed only the presence of pyrite phase, while in the Permian sample the dominance of mixed Fe containing carbonates was observed;
- In the case of mixed carbonates, the metal ratio was determined;
- In the hematite structure, Mn impurity was detected in the case of samples from Urucum deposit and was found to be responsible for the absence of Morin transition.
- According to the Mössbauer results, significant amount of organic anions is assumed to be incorporated into the hematite structure. The organic matter impurity also supports the microbial activity during ore formation.
- Apart from the bulk particles, hematite and manganese nano-oxides (with size-range of a few tens of nanometers) were detected in some samples of the Urucum deposit. Their presence also indicates the microbially mediated formation of these ores.
- New Fe and Mn containing phases of bixbyite $(Mn,Fe)_2O_3$ and hausmannite Mn_3O_4, were identified, while not observed earlier by FTIR and Raman spectroscopies in these samples.

Mössbauer investigations enabled a more detailed novel and independent dataset for the interpretation of the microbially mediated ore formations based on Fe mineralogy.

Declaration of competing interest

The authors declare that they have no known competing financial interests or personal relationships that could have appeared to influence the work reported in this paper.

References

Ashokan, A., Manickavasagam, R.M., Garg, V.K., 1988. Moessbauer and magnetic studies of Jacobsite, in Applications of the Mössbauer Effect, Brazil, pp. 393-396.

Bernard, M.-C., Hugot-Le Goff, A., Thi, B.V., Cordoba de Torresi, S., 1993. Electrochromic reactions in manganese oxides: I. Raman analysis. J. Electrochem. Soc. 140 (11), 3065–3070.

Bessas, D., Sergueev, I., Glazyrin, K., Strohm, C., Kupenko, I., Merkel, D.G., Chumakov, A.I., Rüffer, R., 2020a. On a hyperfine interaction in ε-Fe. Hyperfine Interact. 241 (1), 1–10. https://doi.org/10.1007/s10751-019-1679-3.

Bessas, D., Sergueev, I., Glazyrin, K., Strohm, C., Kupenko, I., Merkel, D.G., Long, G.J., Grandjean, F., Chumakov, A.I., Rüffer, R., 2020b. Revealing the hidden hyperfine interactions in ε-iron. Phys. Rev. B 101 (3), 035112. https://doi.org/10.1103/PhysRevB.101.035112.

Biondi, J.C., Lopez, M., 2017. Urucum Neoproterozoic-Cambrian manganese deposits (MS, Brazil): biogenic participation in the ore genesis, geology, geochemistry, and depositional environment. Ore Geol. Rev. 91, 335–386. https://doi.org/10.1016/j.oregeorev.2017.09.018.

Biondi, J.C., Polgári, M., Gyollai, I., Fintor, K., Kovács, I., Fekete, J., Mojzsis, S.J., 2020. Biogenesis of the Neoproterozoic kremydilite manganese ores from Urucum (Brazil)– a new manganese ore type. Precambr. Res. 340, 105624. https://doi.org/10.1016/j.precamres.2020.105624.

Bødker, F., Mørup, S., 2000. Size dependence of the properties of hematite nanoparticles. EPL (Europhys. Lett.) 52 (2), 217–223. https://doi.org/10.1209/epl/i2000-00426-2.

Cao, M., Qin, K., Li, G., Evans, N.J., Hollings, P., Maisch, M., Kappler, A., 2017. Mineralogical evidence for crystallization conditions and petrogenesis of ilmenite-series I-type granitoids at the Baogutu reduced porphyry Cu deposit (Western Junggar, NW China): Mössbauer spectroscopy, EPM and LA-(MC)-ICPMS analyses. Ore Geol. Rev. 86, 382–403. https://doi.org/10.1016/j.oregeorev.2017.02.033.

da Costa, G.M., Herzog, L.R., 2011. Association between phosphorus and iron oxides in manganese ores. Am. Mineral. 96 (1), 68–73. https://doi.org/10.2138/am.2011.3585.

Dormann, J.L., Djega-Mariadassou, C., Yanev, Y., Renaudin, P., 1989. Mössbauer study of mineral glasses: East rhodope perlites. Hyperfine Interact. 46 (1-4), 651–658. https://doi.org/10.1007/BF02398255.

Frankel, R.B., Blakemore, R.P., 1984. Precipitation of Fe3O4 in magnetotactic bacteria. Philos. Trans. R. Soc. Lond. B Biol. Sci. 304 (1121), 567–574. https://doi.org/10.1098/rstb.1984.0047.

Gracheva, M.A., Chistyakova, N.I., Antonova, A.V., Rusakov, V.S., Zhilina, T.N., Zavarzina, D.G., 2017. Mössbauer study of iron minerals transformations by Fuchsiella ferrireducens. Hyperfine Interact. 238 (1), 84. https://doi.org/10.1007/s10751-017-1460-4.

Hassan, K.M., 2015. The iron mineralogy of Eocene fossil wood—A Mössbauer study of samples from the Petrified Forest, New Cairo Egypt. Canad. Mineral. 53 (4), 705–716. https://doi.org/10.3749/canmin.1400108.

Johnson, C.E., Glasby, G.P., 1969. Mössbauer effect determination of particle size in microcrystalline iron-manganese nodules. Nature 222 (5191), 376–377. https://doi.org/10.1038/222376a0.

Klencsár, Z., Kuzmann, E., Vértes, A., 1996. User-friendly software for Mössbauer spectrum analysis. J. Radioanal. Nucl. Chem. 210 (1), 105–118. https://doi.org/10.1007/bf02055410.

Konhauser, K.O., 1998. Diversity of bacterial iron mineralization. Earth Sci. Rev. 43 (3–4), 91–121. https://doi.org/10.1016/S0012-8252(97)00036-6.

Kuzmann, E., Nagy, S., Vértes, A., Weiszburg, T.G., Garg, V.K., 1998. In: Nuclear Methods in Mineralogy and Geology. Springer US, Boston, MA, pp. 285–376. https://doi.org/10.1007/978-1-4615-5363-2_7.

Lenhart, J.J., Heyler, R., Walton, E.M., Mylon, S.E., 2010. The influence of dicarboxylic acid structure on the stability of colloidal hematite. J. Colloid Interface Sci. 345 (2), 556–560. https://doi.org/10.1016/j.jcis.2010.02.037.

Lin, J.F., Gavriliuk, A.G., Sturhahn, W., Jacobsen, S.D., Zhao, J., Lerche, M., Hu, M., 2009. Synchrotron Mossbauer spectroscopic study of ferropericlase at high pressures and temperatures. Am. Mineral. 94 (4), 594–599. https://doi.org/10.2138/am.2009.3108.

Lipka, J., 1999. Mössbauer Spectroscopy in Mineralogy and Geology. In Mössbauer Spectroscopy in Materials Science. Springer, Dordrecht. pp. 97-106. https://doi.org/10.1007/978-94-011-4548-0_10.

de Medeiros, S.N., Luciano, A., Cótica, L.F., Santos, I.A., Paesano Jr, A., da Cunha, J.B.M., 2004. Structural and magnetic characterization of the ball-milled α-Fe2O3–Mn2O3 and α-Fe–Mn2O3 systems. J. Magn. Magn. Mater. 281 (2–3), 227–233. https://doi.org/10.1016/j.jmmm.2004.04.109.

McCammon, C., Kantor, I., Narygina, O., Rouquette, J., Ponkratz, U., Sergueev, I., Mezouar, M., Prakapenka, V., Dubrovinsky, L., 2008. Stable intermediate-spin ferrous iron in lower-mantle perovskite. Nat. Geosci. 1 (10), 684–687. https://doi.org/10.1038/ngeo309.

Merkel, D.G., Bottyán, L., Tanczikó, F., Zolnai, Z., Nagy, N., Vértesy, G., Waizinger, J., Bommer, L., 2011. Magnetic patterning perpendicular anisotropy FePd alloy films by masked ion irradiation. J. Appl. Phys. 109 (12), 124302. https://doi.org/10.1063/1.3596535.

Morgan, J.J., 2005. Kinetics of reaction between O2 and Mn (II) species in aqueous solutions. Geochim. Cosmochim. Acta 69 (1), 35–48. https://doi.org/10.1016/j.gca.2004.06.013.

Murad, E., Schwertmann, U., 1986. Influence of Al substitution and crystal size on the room-temperature Mössbauer spectrum of hematite. Clays Clay Miner. 34 (1), 1–6. https://doi.org/10.1346/CCMN.1986.0340101.

Pédrot, M., Le Boudec, A., Davranche, M., Dia, A., Henin, O., 2011. How does organic matter constrain the nature, size and availability of Fe nanoparticles for biological reduction? J. Colloid Interface Sci. 359 (1), 75–85. https://doi.org/10.1016/j.jcis.2011.03.067.

Polgári, M., Gyollai, I., Fintor, K., Horváth, H., Pál-Molnár, E., Biondi, J.C., 2019. Microbially mediated ore-forming processes and cell mineralization. Front. Microbiol. 10, 2731. https://doi.org/10.3389/fmicb.2019.02731.

Polgári, M., Biondi, J.C., Gyollai, I., Fintor, K., Szabó, M. (2021). Fe-rich rocks from Urucuat – evidence of microbial origin (Mato Grosso do Sul – Brazil) (submitted to recent volume).

Reeder, R.J., Dollase, W.A., 1989. Structural variation in the dolomite-ankerite solid-solution series; an X-ray, Moessbauer, and TEM study. Am. Mineral. 74 (9–10), 1159–1167.

Shiley, R.H., Cluff, R.M., Dickerson, D.R., Hinckley, C.C., Smith, G.V., Twardowska, H., Saporoschenko, M., 1981. Correlation of natural gas content to iron species in the New Albany shale group. Fuel 60 (8), 732–738. https://doi.org/10.1016/0016-2361(81)90228-3.

Srivastava, J.K., Sharma, R.P., 1972. Magnetic dilution effects on Morin phase transition in hematite. Phys. Status Solidi (b) 49 (1), 135–146. https://doi.org/10.1002/pssb.2220490112.

Stevens, J.G., Khasanov, A.M., Miller, J.W., Pollak, H., Li, Z., 1998. Mossbauer mineral handbook. Mossbauer Effect Data Center, North Carolina.

Tanczikó, F., Bottyán, L., Deák, L., Merkel, D.G., Nagy, D.L., 2009. Sign determination of the hyperfine field by elliptically polarized Mössbauer source. Hyperfine Interact. 188 (1–3), 79–84. https://doi.org/10.1007/s10751-008-9892-5.

Vandenberghe, R.E., De Grave, E., De Geyter, G., Landuydt, C., 1986. Characterization of goethite and hematite in a Tunisian soil profile by Mössbauer spectroscopy. Clays Clay Miner. 34 (3), 275–280. https://doi.org/10.1346/CCMN.1986.0340307.

Weihe, S.H.C., Mangayayam, M., Sand, K.K., Tobler, D.J., 2019. Hematite crystallization in the presence of organic matter: impact on crystal properties and bacterial dissolution. ACS Earth Space Chem. 3 (4), 510–518. https://doi.org/10.1021/acsearthspacechem.8b00166.

Yu, W., Polgári, M., Gyollai, I., Fintor, K., Szabó, M., Kovács, I., Fekete, J., Du, Y., Zhou, Q., 2019. Microbial metallogenesis of Cryogenian manganese ore deposits in South China. Precambr. Res. 322, 122–135. https://doi.org/10.1016/j.precamres.2019.01.004.

Yu, W., Polgári, M., Fintor, K., Gyollai, I., Huang, H., Szabó, M., Du, Y., 2021. Microbial metallogenesis of Early Carboniferous manganese deposit in central Guangxi, South China. (Submitted to recent volume).

Yu, W., Gyollai, I., Fintor, K., Szabó, M., Velledits, F., Polgári, M., 2021b. Metallogenesis of Middle Permian manganese ores. Xinglong, North Guizhou, South China (Submitted to recent volume).

Zaki, M.I., Hasan, M.A., Pasupulety, L., Kumari, K., 1997. Thermochemistry of manganese oxides in reactive gas atmospheres: probing redox compositions in the decomposition course MnO2→ MnO. Thermochim. Acta 303 (2), 171–181.

Zavarzina, D.G., Gavrilov, S.N., Chistyakova, N.I., Antonova, A.V., Gracheva, M.A., Merkel, A.Y., Perevalova, A.A., Chernov, M.S., Zhilina, T.N., Bychkov, A.Y., Bonch-Osmolovskaya, E.A., 2020. Syntrophic growth of alkaliphilic anaerobes controlled by ferric and ferrous minerals transformation coupled to acetogenesis. ISME J. 14 (2), 425–436. https://doi.org/10.1038/s41396-019-0527-4.